J. Fluid Mech. (1985), *vol.* 152, *pp.* 67–81
Printed in Great Britain

Observation and analysis of the Mach reflection of weak uniform plane shock waves. Part 2. Analysis

By J. M. DEWEY AND D. J. McMILLIN
University of Victoria, Victoria, B.C., Canada V8W 2Y2

(Received 7 February 1984)

A non-stationary approach to the reflection of weak plane shocks is suggested as an alternative to the usual pseudo-stationary transformation. For regular reflection the non-stationary model produces results which are identical to those obtained using the pseudo-stationary assumption, but with simpler algebra. For weak Mach reflections, where the predictions of the pseudo-stationary model are in disagreement with experimental results, the non-stationary model predicts accurately the observed shapes and positions of the reflected and Mach stem shocks and the spatially varying flow properties behind these shocks. However, the non-stationary model predicts that the gas flows above and below the contact surface, relative to the triple point, are not quite parallel. Parallel flows could be obtained only in the limiting case of grazing incidence, when the reflected shock was sonic. The model is based on the experimental results presented in Part 1 of this paper.

1. Introduction

Extensive reviews of the literature dealing with the reflection of shock waves at concave corners have been given by several authors (Henderson & Lozzi 1975, 1979; Henderson & Siegenthaler 1980; Henderson 1980; Ben-Dor & Glass 1978, 1979). Most of the studies discussed in these reviews describe the regular and Mach reflection of plane shocks from oblique surfaces in a manner first proposed by von Neumann (1943), in which the non-stationary flow is made pseudo-stationary by superposing on the flow-field a velocity equal and opposite to that of some point attached to the shock front system. For weak incident shocks the theory has not been successful at predicting the angle of incidence at which the transition from regular to Mach reflection occurs, or the angles made by the shocks and the contact surface where they meet at the triple point. The experimental results presented in Part 1 (Dewey & McMillin 1985) of this paper include measurements of the particle velocity vectors throughout the flow field of a weak Mach reflection and permit both a closer look at the limitations of the pseudo-stationary approach and an evaluation of an alternative, non-stationary model.

2. The pseudo-stationary description of shock reflections

Shock reflections can be studied in the laboratory in two ways. If a supersonic wind tunnel is available, an object placed in the flow will produce a bow shock which can be made to interact with a surface to produce a regular or a Mach reflection, depending on the shock strength and the angle of incidence. Such a configuration, as described for example by Hornung & Robinson (1982), produces a stationary reflection pattern which can be studied over an extended period of time, but the

experimental facility required is relatively elaborate and expensive. For this reason most workers have found it more convenient to study shock reflection phenomena using a non-stationary shock produced in a shock tube or similar device. However, in a shock tube the phenomenon lasts for only a fraction of a millisecond, and it is more difficult to describe theoretically a system of moving shocks growing with time.

In an attempt to overcome this last difficulty, self-similarity of the growing shock configuration is assumed and the experimentally observed non-stationary flow is made pseudo-stationary by imposing onto the flow-field a velocity equal and opposite to that of the point of reflection in the case of regular reflection, or of the triple point in the case of Mach reflection. After such a transformation a reflection in a shock tube might be expected to be identical to the corresponding reflection observed in a wind tunnel.

Regular reflection is illustrated in figure 1, in the stationary and pseudo-stationary frames of reference. The incident shock has a Mach number M_1. To bring the shocks to rest, a velocity equal and opposite to that of the reflection point G is imposed on the system. In the resulting pseudo-stationary frame of reference there is an incident oblique flow of Mach number M_0, equal to M_G, through the incident shock. This flow is deflected through an angle θ_1 and the flow speed is reduced to M_1, with a component directed towards the reflecting surface. To conserve mass, the flow through the reflected shock must be oblique and redirected parallel to the reflecting surface, that is, the second deflection angle θ_2 must be equal and opposite to θ_1. The flow velocity is reduced finally to M_2.

Oblique shock theory, as discussed for example by Liepmann & Roshko (1957), shows that there is a maximum possible flow deflection for a shock of a particular strength and that if the angle of the reflecting surface, θ_W in figure 1, is decreased, this maximum deflection angle is eventually reached. At some angle of incidence, therefore, regular reflection must change to Mach reflection.

In the case of Mach reflection, illustrated in figure 2, the non-stationary flow is made pseudo-stationary by imposing a velocity equal and opposite to that of the triple point. The resulting incident flow with Mach number M_0 equal to M_T passes obliquely through the incident shock and is deflected through an angle θ_1. The flow is then deflected by the reflected shock through an angle θ_2, which is less than θ_1. The incident flow also passes through the Mach stem shock and is deflected through an angle θ_3 such that $\theta_3 = \theta_1 - \theta_2$, i.e. the flows on both sides of the contact surface are parallel, though of different speeds. The density and entropy also differ across the contact surface, but the hydrostatic pressure on both sides is the same.

The flows produced by regular and Mach shock reflections in a pseudo-stationary frame are frequently considered using pressure-deflection (P, θ) shock polars. A shock polar is an expression of the relationship, for a given shock strength, between the pressure jump across the shock and the flow deflection. Figure 3 shows the shock polars for a regular reflection. The M_0 and M_1 polars describe the flows through the incident and reflected shocks respectively. The latter has its origin on the former. Pressure in the flow behind the reflected shock relative to that ahead of the incident shock is represented by the point at which the M_1 polar cuts the pressure axis, since the net deflection of the flow is zero.

Figure 4 shows the shock polars for a Mach reflection. The reflected shock polar M_1 has its origin at (P_1, θ_1) on the incident shock polar M_0, corresponding to the conditions behind the incident shock, and it again cuts the M_0 polar at a point which represents both the conditions behind the reflected shock $(P_2, \theta_1 - \theta_2)$ and behind the Mach stem shock (P_3, θ_3).

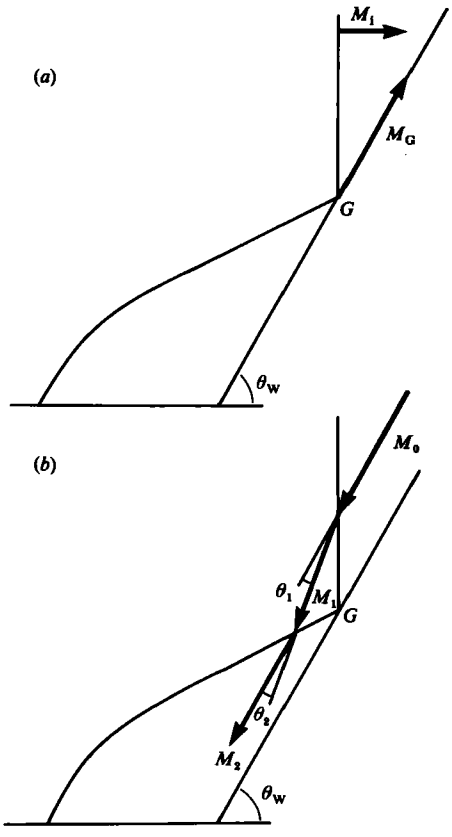

FIGURE 1. Regular reflection of a plane shock at a concave corner (*a*) in the laboratory frame and (*b*) in the pseudo-stationary frame of the reflection point *G*.

3. Failure of the pseudo-stationary model in the case of weak shocks

It is a well-known paradox that the approach of von Neumann succeeds in describing regular reflection and the Mach reflection of strong shocks, but fails to describe the Mach reflection of weak shocks. For weak shocks, the theory fails to predict correctly the angle of incidence at which transition from regular to Mach reflection occurs and, for weak Mach reflection, it fails to predict correctly the angles defined by the shocks and contact surface where they meet at the triple point. The mechanism of transition from regular to Mach reflection in the weak shock case is a continuing problem, but it is not a concern of the present paper.

For most workers using schlieren photography the only flow direction which can be measured is that identified by the contact surface. However, the technique described in Part 1 of this paper has provided a complete mapping of the particle trajectories throughout the flow-field produced by a Mach reflection, so that it is possible to measure the angles of deflection of the flow passing through the curved reflected and Mach stem shocks.

The experimentally determined flows were made pseudo-stationary by imposing on the flow vector field a velocity equal and opposite to that of the triple point. A result for one experiment is shown as figure 5. The flow deflection angles across the

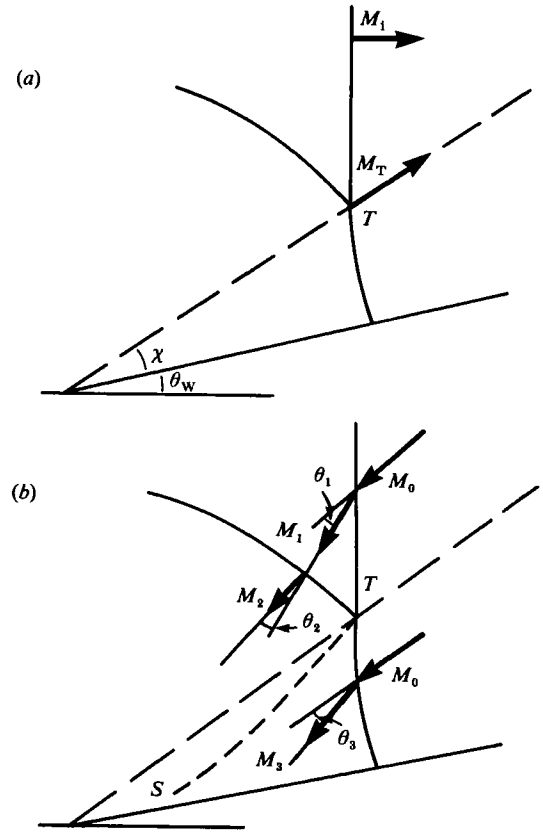

FIGURE 2. Mach reflection of a plane shock at a concave corner (*a*) in the laboratory frame and (*b*) in the pseudo-stationary frame of the triple point T.

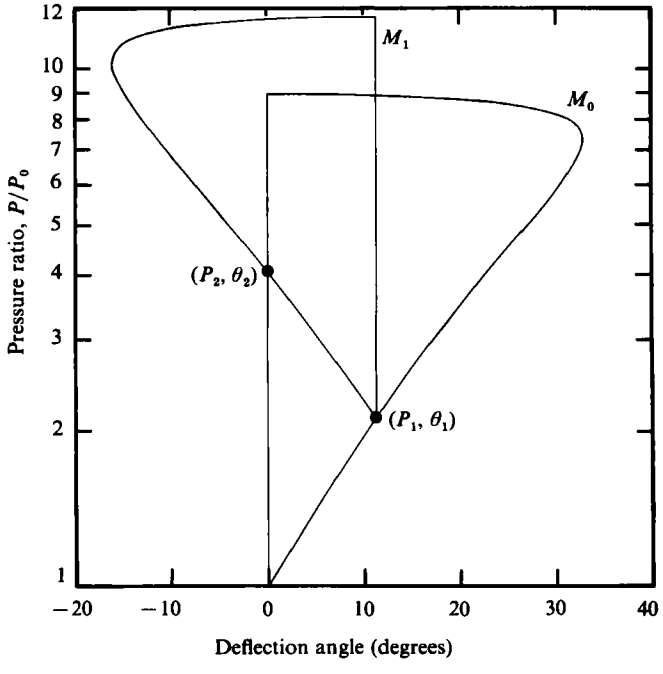

FIGURE 3. The shock polar representation of a particular regular reflection ($M_1 = 1.4$, $\theta_W = 60°$).

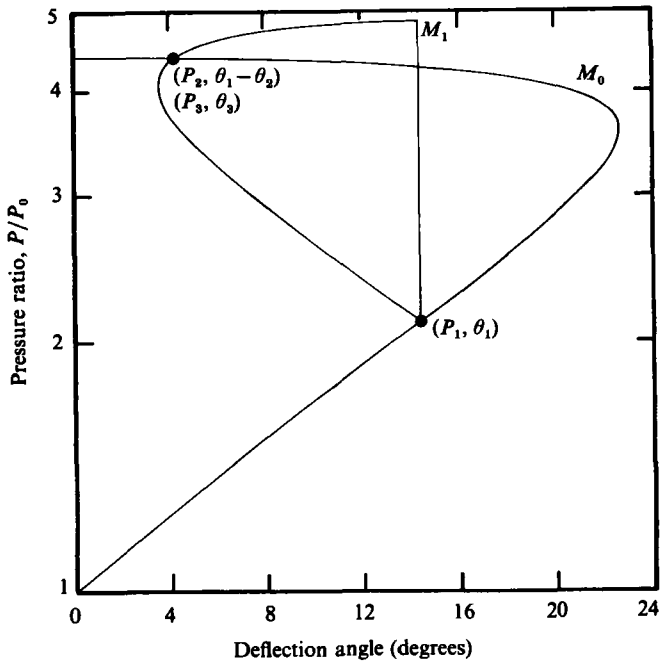

FIGURE 4. The shock polar representation of a Mach reflection ($M_1 = 1.4$, $\chi+\theta_W = 45°$). The relative size of the reflected shock polar, M_1, decreases as the wedge angle θ_W is decreased.

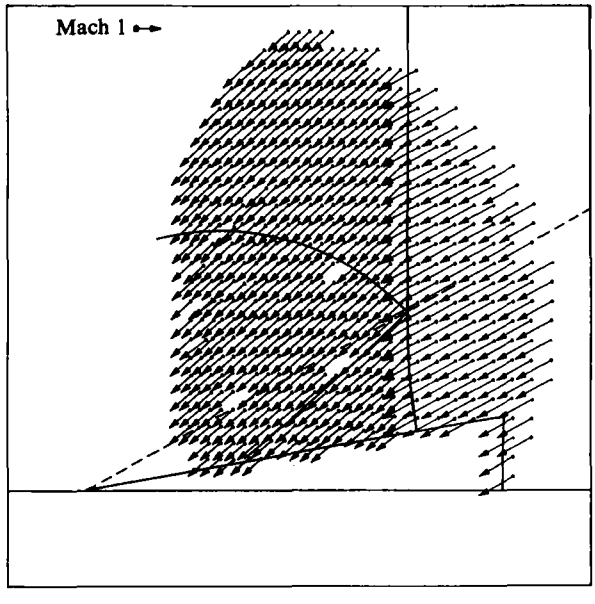

FIGURE 5. Flow in one of the experiments from series 3, in the pseudo-stationary frame of reference of the triple point. The triple-point trajectory in the laboratory frame is shown as a dashed line.

incident, reflected and Mach shocks were determined, and in the subsequent analysis the values of these parameters, measured as close as possible to the triple point, will be discussed. The pressure ratios across the shocks are not changed by the transformation, and are obtained directly from measurements of normal shock speeds as discussed in Part 1. The measured flow velocities, deflection angles and pressures close to the triple point for the three experiments described in Part 1 are given in table 1.

The results from table 1 were used to calculate the shock polars for the three experiments and these are shown in figure 6. The measured conditions across the incident shocks agree with oblique shock theory within the range of experimental variation, i.e. the measured values of P_1 and θ_1 lie on the incident shock polar, and this point was used as the origin for the reflected shock polar. For each experiment the reflected shock polar was small, because the reflected shock is almost sonic in the region behind the incident shock, and as a result these polars do not intersect the incident polars.

In addition, we find that the measured values of P_2 and $\theta_1 - \theta_2$ behind the reflected shock, and of P_3 and θ_3 behind the Mach stem shock do not lie on either the incident or the reflected shock polar. The measured values lie within the rectangles shown in figure 6. The sizes of the rectangles represent the maximum possible deviations that can be obtained using any interpretation of the experimental results. As discussed in Part 1, the angles $\theta_1 - \theta_2$ and θ_3 determined from flow tracer velocities near the triple point are not in agreement with the measured slope of the contact surface at the triple point in experimental series 3, the only series in which the contact surface could be photographically identified. The range of the latter measurements is also plotted in figure 6, as a dashed rectangle. It must be concluded that an accurate estimate of the flow and contact surface angles at the triple point cannot be obtained easily using either the von Neumann theory or experiment, in the case of weak shock reflection at large angles of incidence.

Attempts have been made previously to overcome these difficulties by modifying the von Neumann theory for weak shocks by creating a microstructure in the triple-point region, with the introduction of Prandtl–Meyer expansion waves (Bargmann & Montgomery 1945; Gurderley 1953) and the inclusion of viscous effects (Sternberg 1959). These changes have complicated the theory without achieving agreement with experimental results. The requirement remains for a simple model based on assumptions that have not been invalidated experimentally, the most important of which are the assumptions of two-dimensional, self-similar flow and the validity of oblique shock theory and its use of the Rankine–Hugoniot relations. Real gas effects and viscosity should not be important in the weak shock case, except on a microscale.

For weak Mach reflections, the cross-sections of the shock fronts are generally not straight lines. In the experiments referred to here, both the reflected and Mach stem shocks were circular in cross-section. When the triple point is brought to rest in accordance with the pseudo-stationary model, the growth of these curved shocks appears as a rotation. Both rotations are in a direction such that, at a finite distance from the triple point, the reflected shock is stronger than it would be if it were straight and the Mach stem is weaker. Only the flow through a singular triple point and exactly along an infinitely thin contact surface is truly pseudo-stationary. Neither does transformation of the flow relative to any other point produce a pseudo-stationary flow. For example, transformation of the flow relative to the foot of the Mach stem produces a pseudo-stationary flow only for the streamline along the wedge surface. A Mach reflection for shock strengths in the range being considered, *viz* Mach 1.1

	Series 1		Series 2		Series 3	
	Model	Expt	Model	Expt	Model	Expt
M_i†	1.105	1.105±0.001	1.240	1.240±0.002	1.415	1.415±0.002
$\chi+\theta_W$†	21.95	21.95±0.13	27.00	27.00±0.09	28.98	28.98±0.11
M_1	1.005	1.001±0.005	1.008	1.013±0.006	1.012	1.012±0.013
θ_1	3.439	3.32±0.17	8.717	8.41±0.43	14.56	14.26±0.74
P_1/P_0	1.258	1.265±0.027	1.627	1.627±0.051	2.169	2.183±0.094
$\theta_1-\theta_2$	‡	2.75±0.14	‡	7.50±0.13	‡	13.46±0.08
P_2/P_0	‡	1.273±0.048	‡	1.685±0.061	‡	2.304±0.094

† M_i and $\chi+\theta_W$ are the input parameters to the model.

‡ The pseudo-stationary model does not predict any values of P_2/P_0 and $\theta_1-\theta_2$ which are distinct from P_1/P_0 and θ_1, that is, there is no intersection of the polars shown in figure 6 other than the origin of the M_1 polar.

TABLE 1. Flow properties near the triple point computed using the pseudo-stationary model, compared with values measured experimentally

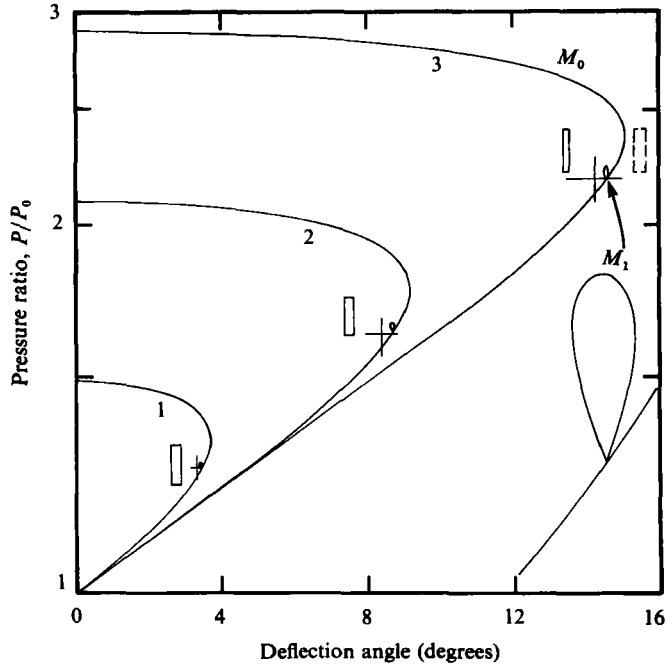

FIGURE 6. Incident and reflected shock polars computed for the three experimental series described in Part 1 of this paper. The reflected shock polar for series 3 is also shown enlarged. The flow deflections and pressures measured behind the incident shocks are represented by crosses and those behind the reflected shocks near the triple point are represented by rectangles. Contact surface angles measured at the triple point in series 3 are represented by the dashed rectangle.

to 1.4, can be made truly pseudo-stationary only by superimposing a very complex flow-field such as that indicated by Jones, Martin & Thornhill (1951). This conclusion may not be true for stronger shocks. At shock strengths for which the reflected and Mach stem shocks are straight in the region of the triple point, the pseudo-stationary assumption is appropriate.

4. A non-stationary description of shock reflections

If the flow associated with a weak Mach reflection cannot be made pseudo-stationary by a simple transformation, it is appropriate to look for an alternative method of describing such a flow. The ideal description of the flow would use as input parameters only the initial state of the gas, the strength of the incident shock and the angle of inclination of the reflecting surface. From these parameters alone, however, it is difficult to compute the strength of the reflected shock in a Mach reflection and so, to obtain the reflected shock strength in the later analysis, the observed value for the triple-point trajectory angle is also included as an input parameter.

4.1. *Non-stationary regular reflection at a small angle of incidence*

To evaluate the non-stationary approach it was first applied to regular reflection at a small angle of incidence, for which the pseudo-stationary approach is known to produce valid results.

Figure 7 represents the regular reflection of a plane shock from a rigid smooth surface at an angle of incidence ω_1, such that the signal from the corner 0 does not overtake the reflected shock at the point of reflection G. The reflected shock is therefore planar near G. The incident shock Mach number is M_i and the pressure, density and sound speed of the gas ahead of the incident shock are P_0, ρ_0, and c_0, respectively.

The particle velocity, u_1, and sound speed, c_1, behind the incident shock are given by the normal shock relations:

$$\frac{u_1}{c_0} = \frac{2}{\gamma+1}\left(M_i - \frac{1}{M_i}\right), \tag{1}$$

and

$$\frac{c_1}{c_0} = \left[\frac{[\gamma M_i^2 - \tfrac{1}{2}(\gamma-1)][\tfrac{1}{2}(\gamma-1)M_i^2+1]}{[\tfrac{1}{2}(\gamma+1)]^2 M_i^2}\right]^{\frac{1}{2}}, \tag{2}$$

where γ is the ratio of specific heats.

If M_r' is the Mach number of the reflected shock in the frame of the gas moving behind the incident shock, then the particle velocity behind the reflected shock in this frame is $\boldsymbol{u}_2' = \boldsymbol{u}_2 - \boldsymbol{u}_1$, where

$$\frac{u_2'}{c_1} = \frac{2}{\gamma+1}\left(M_r' - \frac{1}{M_r'}\right). \tag{3}$$

Also, if $\boldsymbol{u}_2$ is parallel to the reflecting surface,

$$\frac{u_2'}{\sin\theta_W} = \frac{u_1}{\sin(90-\omega_r)}, \tag{4}$$

where ω_r is the angle of reflection and θ_W is the inclination of the reflecting surface ($\theta_W = 90-\omega_i$).

Combining (3) and (4), we may write

$$\frac{u_1\cos\omega_i}{c_1\cos\omega_r} = \frac{2}{\gamma+1}\left(M_r' - \frac{1}{M_r'}\right). \tag{5}$$

The point of reflection, G, lies on the reflecting surface and on the incident and reflected shocks. The velocity of this point along the reflecting surface can therefore be written

$$V_G = V_r \operatorname{cosec}\omega_r = V_i \operatorname{cosec}\omega_i, \tag{6}$$

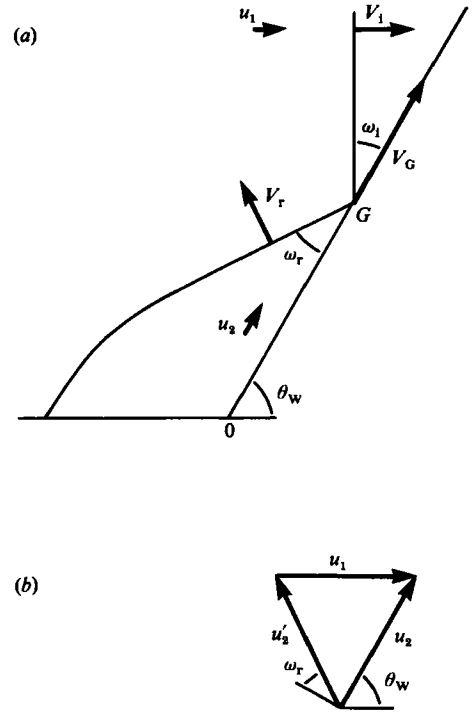

FIGURE 7. (*a*) Definition of the variables and (*b*) a vector relationship, used in the non-stationary model for regular reflection.

where V_r and V_i are speeds of the reflected and incident shocks, respectively. V_r is also equal to the speed of the reflected shock relative to the gas behind the incident shock V_r' less the component perpendicular to the reflected shock of the particle velocity behind the incident shock, i.e.

$$V_r' = V_r - u_1 \sin(\omega_r - \theta_W). \tag{7}$$

Combining (6) and (7) gives the Mach number of the reflected shock relative to the flow behind the incident shock:

$$M_r' = \frac{V_r'}{c_1} = \frac{c_0}{c_1} M_i \frac{\operatorname{cosec}\omega_i}{\operatorname{cosec}\omega_r} - \frac{u_1}{c_1} \sin(\omega_r - \theta_W), \tag{8}$$

which, together with (5), gives

$$\frac{u_1 \cos\omega_i}{c_1 \cos\omega_r} = \frac{2}{\gamma+1} \left[\frac{c_0}{c_1} M_i \frac{\operatorname{cosec}\omega_i}{\operatorname{cosec}\omega_r} - \frac{u_1}{c_1} \sin(\omega_r - \theta_W) - \frac{1}{\frac{c_0}{c_1} M_i \frac{\operatorname{cosec}\omega_i}{\operatorname{cosec}\omega_r} - \frac{u_1}{c_1} \sin(\omega_r - \theta_W)} \right]. \tag{9}$$

This last equation may be rewritten as

$$EF \tan^3\omega_r - (EG + F^2 - 1) \tan^2\omega_r + (EF + 2FG) \tan\omega_r - (EG + G^2 + 1) = 0,$$

where E, F and G are all functions of the initial parameters M_i and ω_i after application of (1) and (2).

The angle of reflection obtained from the numerical solution of (9) may be put into (5) to obtain the strength of the reflected shock, M_r', which in turn gives the pressure, P_2, and the particle velocity, u_2', behind the reflected shock. The particle velocity behind the reflected shock in the fixed frame of reference is obtained using the vector relation $\boldsymbol{u}_2 = \boldsymbol{u}_2' + \boldsymbol{u}_1$, where $\boldsymbol{u}_1$ is the particle velocity behind the incident shock computed using the normal shock equations.

Solutions were obtained for incident shock strengths ranging from $\xi = 0.1$ to 0.9, where ξ is the inverse pressure ratio P_0/P_1 across the shock, and angles of incidence throughout the range for which a real solution is possible. The relationships between angle of incidence and angle of reflection, between incident and reflected shock strengths, and the extreme angles of incidence for which a solution was possible agreed exactly with these relationships calculated by Polachek & Seeger (1951), who used the pseudo-stationary approach. It is known that there is good agreement between the Polachek & Seeger solutions and experimental results, except in the region close to the extreme angle of incidence when the corner signal begins to overtake the point of reflection. It has, therefore, been demonstrated that the non-stationary approach described here duplicates the pseudo-stationary results for regular reflection, and with much simpler algebraic manipulation.

4.2. *Mach reflection at large angles of incidence*

With the establishment of the validity of the non-stationary approach in the case of regular shock reflection at small angles of incidence, the same approach was applied to Mach reflection at large angles of incidence, for the range of shock strengths and the small wedge angle used in the experiments described in Part 1. On the basis of the experimental observations, it is assumed that the cross-section of the reflected shock is circular, centred on a point which moves with the velocity of the flow behind the incident shock, and that the cross-section of the Mach stem shock is circular and perpendicular to the reflecting surface.

The shock configuration is shown in figure 8. The aim is to describe this configuration in terms of the incident shock Mach number, M_i, the wedge angle, θ_W, and the rest gas conditions ahead of the incident and Mach stem shocks. Particle velocity and sound speed behind the incident shock are given by (1) and (2).

With the assumption of circularity of the reflected shock, its speed, relative to the flow behind the incident shock, is given by

$$V_r'^2 = u_1^2 + V_T^2 - 2u_1 V_T \cos(\chi + \theta_W), \tag{10}$$

where V_T is the speed of the triple point, and χ is the angle between the triple-point trajectory and the reflecting surface. V_T may be obtained from the incident shock speed using

$$V_T = V_i \sec(\chi + \theta_W). \tag{11}$$

The Mach number of the reflected shock relative to the flow behind the incident shock, $M_r' = V_r'/c_1$, can therefore be obtained from (10) and (11) in terms of the triple-point trajectory angle, χ.

The pressure ratios across the incident and reflected shocks are given by the normal shock relations

$$\frac{P_1}{P_0} = \frac{2\gamma M_i^2 - (\gamma - 1)}{\gamma + 1} \tag{12}$$

and

$$\frac{P_2}{P_1} = \frac{2\gamma M_r'^2 - (\gamma - 1)}{\gamma + 1} \tag{13}$$

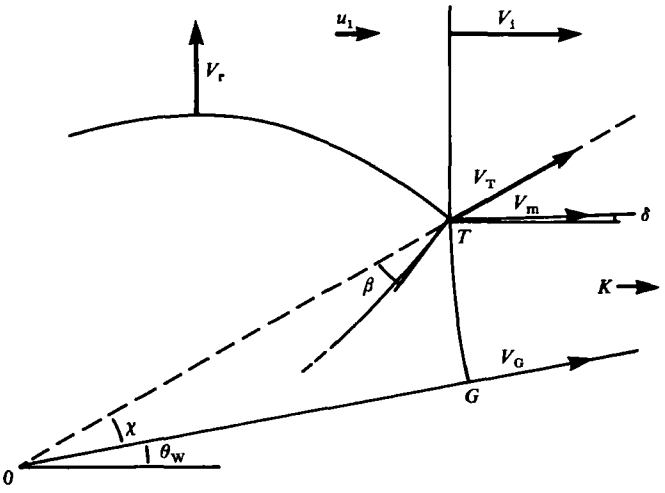

FIGURE 8. Definition of the variables used in the non-stationary model for Mach reflection.

so that
$$\frac{P_2}{P_0} = \frac{[2\gamma M_r'^2 - (\gamma-1)][2\gamma M_1^2 - (\gamma-1)]}{(\gamma+1)^2}. \tag{14}$$

Similarly, the pressure ratio across the Mach stem just below the triple point in terms of its speed there, M_m, is
$$\frac{P_3}{P_0} = \frac{2\gamma M_m^2 - (\gamma-1)}{\gamma+1}. \tag{15}$$

Since the pressures on both sides of the contact surface are equal, (14) and (15) give
$$2\gamma M_m^2 - (\gamma-1) = \frac{[2\gamma M_r'^2 - (\gamma-1)][2\gamma M_1^2 - (\gamma-1)]}{\gamma+1}. \tag{16}$$

This equation gives M_m in terms of M_r', and thus in terms of the triple-point trajectory angle, χ. As the triple point lies on both the incident and Mach stem shocks, it can also be expressed in terms of χ and δ, the acute angle between the two shocks:
$$M_m = \frac{M_1 \cos(\chi+\theta_w-\delta)}{\cos(\chi+\theta_w)}. \tag{17}$$

The flow velocity behind the Mach stem at the triple point, u_3, has a direction defined by δ and magnitude given by the normal shock relation
$$\frac{u_3}{c_0} = \frac{2}{\gamma+1}\left(M_m - \frac{1}{M_m}\right). \tag{18}$$

The particle velocity behind the reflected shock in the stationary frame is $\boldsymbol{u}_2$, and relative to the flow behind the incident shock, $\boldsymbol{u}_2' = \boldsymbol{u}_2 - \boldsymbol{u}_1$. The normal shock relations give the magnitude of u_2' in terms of M_r':
$$\frac{u_2'}{c_1} = \frac{2}{\gamma+1}\left(M_r' - \frac{1}{M_r'}\right). \tag{19}$$

Let $\boldsymbol{u}_2$ at the triple point, just above the slipstream, be oriented at an angle α above the horizontal, as shown in figure 9. Then
$$\frac{u_1}{\sin(\psi-\alpha)} = \frac{u_2'}{\sin\alpha} = \frac{u_2}{\sin\psi}, \tag{20}$$

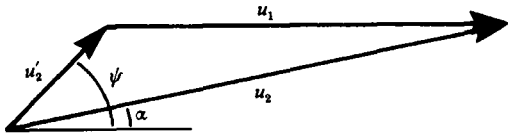

FIGURE 9. Vector relationship between the particle flows in the Mach reflection model.

where ψ is the angle of inclination of the radius vector of the reflected shock through the triple point, defined by

$$\tan\psi = \frac{V_1 \tan(\chi+\theta_W)}{V_1-u_1}. \tag{21}$$

From (20) both u_2 and α, the magnitude and direction of the flow behind the reflected shock, are obtained in terms of χ.

The inclination of the slipstream can be obtained by considering the flow on the two sides of the contact surface, relative to the triple point. The vector diagram for the flow behind the Mach stem shock is shown as figure 10, from which

$$\frac{u_3}{\sin\beta_3} = \frac{V_T}{\sin(\chi+\theta_W+\beta_3-\delta)}, \tag{22}$$

from which in turn β_3, the angle between the slipstream and the triple-point trajectory, can be determined in terms of χ. A similar relationship can be applied to the flow behind the reflected shock:

$$\frac{u_2}{\sin\beta_2} = \frac{V_T}{\sin(\chi+\theta_W+\beta_2-\alpha)}. \tag{23}$$

Assuming that the shape of the cross-section of the Mach stem shock is circular and that the Mach stem shock is perpendicular to the reflecting surface, the position of this shock can be derived. Referring back to figure 8, the normal to the Mach stem shock at the triple point is inclined at δ to the incident flow. Let this normal vector intersect the reflecting surface at K. The Mach stem is then represented by a circle of radius TK, centred at K and intersecting the reflecting surface at G. The velocity of G, the foot of the Mach stem, along the reflecting surface is given by

$$V_G = \frac{V_T[\sin(\chi+\theta_W-\delta)-\sin\chi]}{\sin(\theta_W-\delta)}. \tag{24}$$

5. Evaluation of the non-stationary model

The wedge angle and the strengths of the incident shocks of the experiments described in Part 1 were used with (10)–(24) to calculate the shock positions and flow parameters, in terms of the triple-point trajectory angle χ. The values of χ which were measured in the three series of experiments were then applied in the equations and numerical values of the properties calculated. The results gave excellent descriptions of the shock positions, as illustrated in figure 11, and of the flow properties adjacent to the triple point, as listed in table 2.

Differences between the calculated and observed values of particle velocity, u_2 and u_3, and pressure, P_2 and P_3, were within the experimental errors and extremely small, particularly for series 1 and 2 for which the Mach numbers of the incident shocks were 1.105 and 1.240, respectively. There was excellent agreement between the

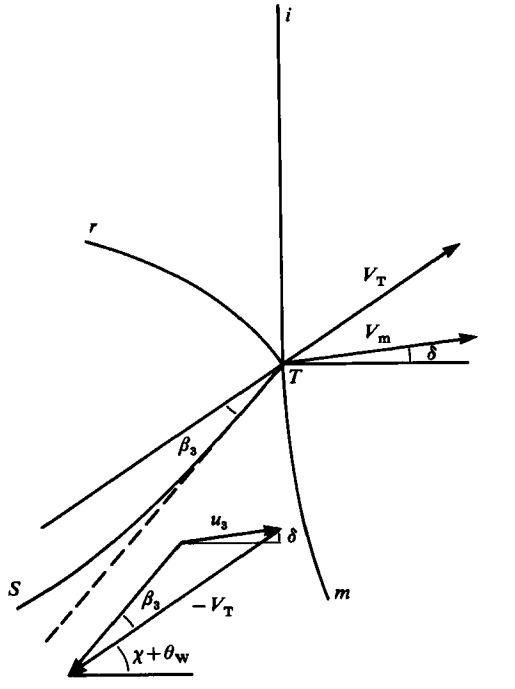

FIGURE 10. Mach stem shock speed and particle flow vectors at the triple point. The slipstream is labelled *S*.

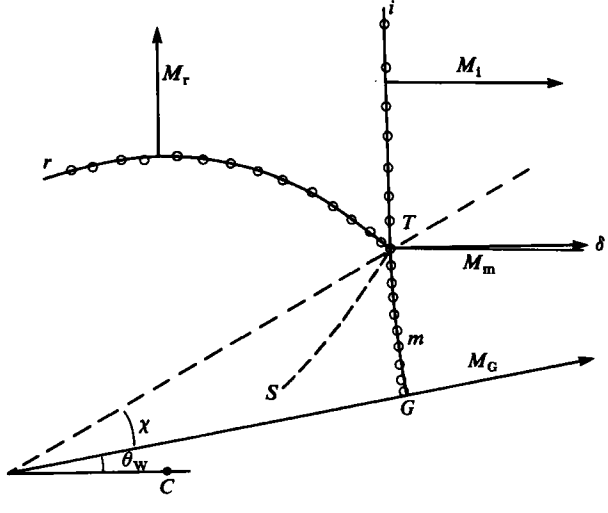

FIGURE 11. A graphical comparison between the shock front configuration as predicted by the non-stationary model and points measured on the shock fronts in photographs, for one of the series 3 experiments ($M_1 = 1.415$, $\chi+\theta_W = 28.98°$). Although there is a small difference between the positions of the Mach stem shock at the wedge surface, *G*, the predicted and measured values of its speed up the wedge were found to be in excellent agreement.

	Series 1		Series 2		Series 3	
	Model	Expt	Model	Expt	Model	Expt
M_1†	1.105	1.105±0.001	1.240	1.240±0.002	1.415	1.415±0.002
$\chi+\theta_w$†	21.95	21.95±0.13	27.00	27.00±0.09	28.98	28.98±0.11
M_r	1.007	1.001±0.005	1.009	1.013±0.006	1.012	1.012±0.013
β_2	3.31	2.75±0.19	8.48	7.50±0.09	14.39	13.46±0.08
β_3	3.45	2.70±0.14	8.68	7.40±0.13	14.65	13.45±0.24
u_2/c_0	0.176	0.179±0.004	0.375	0.372±0.005	0.609	0.615±0.012
u_3/c_0	0.176	0.178±0.004	0.378	0.380±0.005	0.615	0.638±0.010
P_2/P_0	1.269	1.273±0.048	1.643	1.685±0.061	2.211	2.304±0.094
P_3/P_0	1.269	1.278±0.041	1.643	1.663±0.043	2.211	2.322±0.106
M_m	1.111	1.112±0.002	1.252	1.254±0.003	1.435	1.453±0.011
M_G	1.147	1.144±0.003	1.301	1.293±0.003	1.491	1.487±0.003

† M_1 and $\chi+\theta_w$ are the input parameters to the model.

TABLE 2. Flow properties near the triple point computed using the non-stationary model, compared with values measured experimentally

calculated and observed Mach numbers of the Mach stem shocks, both at the triple point, M_m, and at the wedge surface, M_G. The differences between observed and calculated values of M_G were only 0.26 %, 0.31 % and 0.27 % in the three experimental series.

It will be noted from the results listed in table 2 that β_2 and β_3, the angles of the flow velocity vectors above and below the slipstream, relative to the triple point, are not equal. The difference between these angles are small, *viz* 0.14°, 0.20° and 0.26°, but are not caused by numerical inaccuracies in the solution of the equations. If it is assumed that $\beta_2 = \beta_3$, (22) and (23) can be solved for χ, and the model does not then require the input of any measured parameter to define the strength of the reflected shock. Unfortunately this yields the solution for an infinitely thin wedge, with a sonic reflected shock, and for which the strength of the Mach stem shock close to the triple point equals that of the incident shock.

Sternberg (1959) has shown that, when viscosity is considered, the condition that $\beta_2 = \beta_3$ is not required, and also that P_2 will not equal P_3, a basic assumption of the inviscid model. The slight difference between the values of β_2 and β_3 given by the inviscid, non-stationary model may indicate an error in that model's assumptions, such as the circularity of the cross-sections of the reflected and Mach stem shocks, but no such error is apparent in the experimental results.

The differences between the values of β_2 and β_3 obtained from the model and the measured slopes of the contact surfaces, as given in table 2, are probably not significant since the measured values refer to a part of the contact surface about 1.5 cm from the triple point, as explained in Part 1.

6. Conclusions

An analysis of the experimentally observed particle trajectories in the three flow regions defined by a Mach reflection has confirmed that the descrption of the phenomenon based on the assumptions of the classical pseudo-stationary theory is inappropriate for the range of incident shock strengths and the angle of incidence studied in the experiments described in Part 1. An alternative, non-stationary

approach to plane shock reflections has been suggested. In the region of regular reflection this approach produces results which are identical to those using a pseudo-stationary configuration relative to the reflection point, and with simpler algebra. In the case of Mach reflection at large angles of incidence, the non-stationary model gives the shock positions and flow properties behind the reflected and Mach shocks in excellent agreement with measured values.

The model also gives values of the flow properties in regions not immediately adjacent to the triple point, such as the foot of the Mach stem. This would appear to be a necessary feature of any description of the Mach reflection of weak shocks in which the particle and sound speeds are such as to permit signals from the flow-field to overtake the shocks.

The model does not predict parallel flows, relative to the triple point, on the two sides of the slipstream. Parallel flows could be obtained only in the limiting case of a very large angle of incidence in which the reflected shock was sonic.

The authors gratefully acknowledge the assistance of W. Heilig for discussions of shock polar and alternative theories. Financial support for this project was provided by the Defence Research Establishment Suffield; the Natural Sciences and Engineering Research Council of Canada; the Scientific Affairs Division of NATO, and the University of Victoria.

REFERENCES

BARGMANN, V. & MONTGOMERY, D. 1945 O.S.R.D. No. 5011.

BEN-DOR, G. & GLASS, I. I. 1978 *AIAA J.* **16**, 1146.

BEN-DOR, G. & GLASS, I. I. 1979 *J. Fluid Mech.* **92**, 459.

DEWEY, J. M. & MCMILLIN, D. J. 1985 *J. Fluid Mech.* **152**, 49–66.

GURDERLY, K. G. 1947 *Wright Field Report* F-TR-2168-ND.

HENDERSON, L. F. 1980 *J. Fluid Mech.* **99**, 801.

HENDERSON, L. F. & LOZZI, A. 1975 *J. Fluid Mech.* **68**, 139.

HENDERSON, L. F. & LOZZI, A. 1979 *J. Fluid Mech.* **94**, 541.

HENDERSON, L. F. & SIEGENTHALER, A. 1980 *Proc. R. Soc. Lond.* A **369**, 537.

HORNUNG, H. G. & ROBINSON, M. L. 1982 *J. Fluid Mech.* **123**, 155.

JONES, D. M., MARTIN, P. M. E. & THORNHILL, G. K. 1951 *Proc. R. Soc. Lond.* A **209**, 238.

LIEPMANN, H. W. & ROSHKO, A. 1957 *Elements of Gas Dynamics.* Wiley.

NEUMANN, J. VON 1943 See *Collected Works* **6**, 1963 Pergamon, p. 239.

POLACHEK, H. & SEEGER, R. J. 1951 *Phys. Rev.* **84**, 922.

STERNBERG, J. 1959 *Phys. Fluids* **2**, 179.